Parameter Reduction of Composite Load Model Using Active Subspace Method

Zixiao Ma, *Graduate Student Member, IEEE,* Bai Cui, *Member, IEEE,* Zhaoyu Wang, *Senior Member, IEEE,* and Dongbo Zhao, *Senior Member, IEEE*

***Abstract*—Over the past decades, the increasing penetration of distributed energy resources (DERs) has dramatically changed the power load composition in the distribution networks. The traditional static and dynamic load models can hardly capture the dynamic behavior of modern loads especially for fault-induced delayed voltage recovery (FIDVR) events. Thus, a more comprehensive composite load model with combination of static load, different types of induction motors, single-phase A/C motor, electronic load and DERs has been proposed by Western Electricity Coordinating Council (WECC). However, due to the large number of parameters and model complexity, the WECC composite load model (WECC CMLD) raises new challenges to power system studies. To overcome these challenges, in this paper, a cutting-edge parameter reduction (PR) approach for WECC CMLD based on active subspace method (ASM) is proposed. Firstly, the WECC CMLD is parameterized in a discrete-time manner for the application of the proposed method. Then, parameter sensitivities are calculated by discovering the active subspace, which is a lower-dimensional linear subspace of the parameter space of WECC CMLD in which the dynamic response is most sensitive. The interdependency among parameters can be taken into consideration by our approach. Finally, the numerical experiments validate the effectiveness and advantages of the proposed approach for WECC CMLD model.**

***Index Terms*—WECC composite load model, parameter reduction, active subspace, dimension reduction.**

I. Introduction

LOAD modeling is significant for power system studies such as parameter identification, optimization and stability analysis, which has been widely studied [1]. It can be classified into static and dynamic load models. Constant impedance-current-power (ZIP) model, exponential model and frequency dependent model are typical static loads models, and traditional dynamic load models include induction motor (IM) and exponential recovery load model [2]. To provide more accurate responses, composite load models are developed by combining static and dynamic load models. Motivated by the 1996 blackout reported by the Western Systems Coordinating Council (WSCC), the classic ZIP+IM composite load model was developed to model highly stressed loading conditions in summer peak hours [3]. However, this interim load model was unable to capture the fault-induced delayed voltage recovery (FIDVR) events [4]. Therefore, a more comprehensive composite load model was proposed by Western Electricity Coordinating Council (WECC) that contains substation transformer, shunt reactance, feeder equivalent, induction motors, single-phase AC motor, ZIP load, electronic load, and DER [5]. WECC composite load model (WECC CMLD) produces accurate responses, nevertheless, the large number of parameters and high model complexity raise new challenges for power system studies. Name parameter identification as one significant example, where the large number of parameters brings great difficulties to search for global optimum when performing parameter identification. The reason is twofold: firstly, the large number of parameters result in a large search space that reduces the optimization efficiency; secondly, the insensitive parameters and parameter interdependencies usually result in a large number of local optima, which increases the difficulty of achieving global optimum [6]. Although the parameters have physical meanings, some of them only have marginal impacts on the model response altogether or along certain parameter variation directions [7]. Moreover, considering full load model parameter set could significantly increase the complexity of power system studies. Therefore, it is imperative to develop a method to screen out the insensitive parameters. Then, only the sensitive parameters are to be determined in the parameter identification problem while the others can be kept at their respective default values. In this way, the dimension of search space of load model parameters can be significantly reduced. Thus, lower computational cost (less model runs) and higher accuracy (easier to find the optimum) can be achieved when conducting power system studies such as parameter identification without compromising fidelity of the load model.

The above problem can be resolved by dimension reduction in parameter space based on sensitivity analysis of a parameterized model whose inputs are system parameters. As discussed in [8], parameter reduction (PR) methods can be classified into local and global ones. Local PR methods are suitable for known parameters with small uncertainties, in which partial derivatives of output with respect to the model parameters are computed to evaluate the relative variation of output with respect to each parameter. Nonetheless, the input parameters are subject to a range in typical load modeling problems. Therefore, a global sensitivity metric is necessary to measure the sensitivity of output with respect to parameters.

There are many existing global PR approaches. One of

This work was supported in part by Advanced Grid Modeling Program at the U.S. Department of Energy Office of Electricity under Grant DE-OE0000875, and in part by the National Science Foundation under CMMI 1745451. (*Corresponding author: Zhaoyu Wang*)

Z. Ma, and Z. Wang are with the Department of Electrical and Computer Engineering, Iowa State University, Ames, IA 50011, USA (email: zma@iastate.edu; wzy@iastate.edu). (*Corresponding author: Zhaoyu Wang*)

Bai Cui is with National Renewable Energy Laboratory, Golden, CO 80401, USA (email: bcui@nrel.gov).

Dongbo Zhao is with Argonne National Laboratory, Argonne, IL 60439, USA (email: dongbo.zhao@anl.gov).

the most common and simplest techniques in engineering is the so-called "One-At-A-Time" (OAT) method that varies one parameter while fixing the others. However, this method can only provide a rough qualitative approximation of the parameter sensitivities and cannot fully reveal the nonlinearity and interdependency among the parameters due to its low exploration of the parameter space. In [9], the OAT method was improved by proposing two sensitivity measures, mean μ and standard deviation σ based on the elementary effects methods. This method has higher exploration rate of the parameter space and can qualitatively analyze which parameter may have influence on nonlinear and/or interaction effects. This method is further extended by supersaturated design [10], screening by groups [11], sequential bifurcation method [12] and factorial fractional design [13] based on the number of parameters and experiments in a particular scenario [14].

To quantitatively study the comprehensive parameter sensitivity patterns and their interdependencies, variance-based approaches such as Sobel indices [15] were proposed for nonlinear and non-monotonic models. However, to precisely estimate the sensitivity indices with arbitrary order interactions between parameters, these approaches require a formidably large number of experiments [16]. In [17], a total-effect index was introduced, which can measure the contribution to the output variance of parameters, including all variance caused by its interactions of any order with any other parameters, as well as reducing the requirement of the number of experiments. These indices are usually estimated by Monte Carlo methods [18]. Such methods are accurate but suffer from high computational cost when large sample size is required. Thus, it motivates the recent research on exploring efficient numerical algorithms including the analysis of variance (ANOVA) decomposition [19], Fourier Amplitude Sensitivity Test (FAST) [20] and least absolute shrinkage and selection operator (LASSO) [21]. Despite the relative reduction in computational cost by these methods, they can result in instability and inaccuracy when the number of parameters increases (larger than 10) [14], [22]. Some researches delve into the trajectory sensitivity analysis, e.g., in [23], the time-varying parameter sensitivities of ZIP+IM model are derived based on perturbation and Taylor expansion method. However, such methods need explicit mathematical model and require the model output to be differentiable with respect to the parameters for the Jacobian matrices to exist, which makes it inapplicable for WECC CMLD. Different from OAT and and variance-based approaches, the active subspace method (ASM) is based on gradient evaluations for detecting and exploiting the most influential direction in the parameter space of a given model to construct an approximation on a low-dimensional subspace of the model's parameters as well as quantify the interdependencies among parameters [24]. As a Monte Carlo sampling based method, ASM also requires multiple experiments, but it has better accuracy and requires relatively lower sample size.

There are limited studies on the PR problem of WECC CMLD. In [1], the parameter sensitivity and interdependencies among parameters are analyzed using OAT method and clustering techniques, motivated by observing that different parameter combinations can give the same data fitting results in measurement-based load modeling. As discussed above, the OAT method suffers from low accuracy and low exploration rate of the parameter space. Moreover, the interdependency is simply determined by whether parameters have similar trajectory sensitivities in this work. In addition, the newly-approved aggregated distributed energy resources (DER_A) model in WECC CMLD has not been considered. PR was conducted by means of data-driven feature-wise kernelized LASSO (FWKL) in [21], which uses multiple randomly-generated parameter vectors and corresponding output residuals to compute parameter sensitivities by solving a LASSO optimization problem. This approach avoids utilizing analytical gradient and can obtain the optimal sensitivity. In addition, the employment of LASSO ensures parameter interdependency is captured in a feature-wise manner. However, due to high non-convexity of WECC CMLD, the result is very sensitive to parameter setting of the algorithm and the distribution of the dataset. Also, the large number of experiments and optimization process greatly increase its computational cost.

In this paper, a novel PR approach is proposed by leveraging the ASM. As an alternative PR technique, ASM is a relatively new dimension reduction tool that has shown its effectiveness in many fields such as bioengineering [25] and aerospace engineering [26]. The outstanding advantages of ASM include relatively low computational cost, high accuracy and the ability to quantify the parameter interdependency.

The novelty and main contributions of our paper are summarized as follows. Motivated by the fact that the WECC CMLD is a differential-algebraic system and ASM can only deal with algebraic functions, we first cast the WECC CMLD as a discrete-time system for parameterization. Secondly, a comprehensive PR approach tailored for WECC CMLD based on ASM is proposed. Thirdly, factors influencing accuracy of PR results are rigorously analyzed. Finally, statistical and numerical experiments are conducted to validate the effectiveness of the proposed method. Comparative case studies with three classical PR methods are also conducted and discussed.

The rest of the paper is organized as follows. Section II introduces the WECC CMLD and develops its parameterized model. Section III proposes the PR algorithm and conducts accuracy analysis. Case studies are carried out in Section IV to demonstrate the effectiveness of the proposed method, which is followed by conclusions.

II. Problem Statement

In this section, the structure and function of WECC CMLD are introduced, then a parameterized model of the composite load is established for PR.

A. Introduction of WECC CMLD

As shown in Fig. 1, WECC CMLD consists of three 3-phase motors, one single-phase motor, one ZIP load, one electronic load and one DER_A model. Three 3-phase motors represent three different types of dynamic components. Motor A represents three-phase induction motors with low inertia driving constant torque loads, e.g. air conditioning compressor motors and positive displacement pumps. Motor B represents

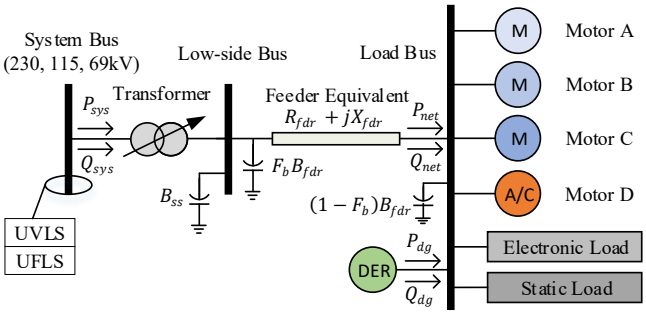

Fig. 1. A schematic diagram of the WECC CMLD [28].

three-phase induction motors with high inertia driving variable torque loads such as commercial ventilation fans and air handling systems. Motor C represents three-phase induction motors with low inertia driving variable torque loads such as the common centrifugal pumps. Single-phase motor D captures behaviors of single-phase air with reciprocating compressors. However, it is challenging to model the fault point-on-wave and voltage ramping effects [5]. Moreover, new A/C motors are mostly equipped with scroll compressors and/or power electronic drives, making their dynamic characteristics significantly different than conventional motors. Therefore, WECC uses a performance-based model to represent single-phase motors. As increasing percentage of end-uses become electronically connected [3], the WECC CMLD adopts a simplistic representation of power electronic loads as constant power loads with unity power factor. A ZIP load is used as static one in this model. The DER model is specified as the newly-approved DER_A model presented in [27].

B. Motivation for PR

The WECC CMLD contains 183 parameters, which pose significant challenges for power system studies such as parameter identification, optimization and control. By observing that part of the parameters can be determined by engineering judgment, we can filter out them according to the analysis in [21]. In particular, the parameters of transformer, feeder, and the stalling and restarting of induction motors can be excluded since they have small range of uncertainties and are usually pre-determined by their default values to meet practical engineering requirements. In this way, 64 parameters are screened out *a priori*. Nonetheless, the number of parameters that remains is still too large for power system studies. Therefore, in this paper, we use ASM to further reduce the number of parameters. The WECC CMLD is a differential-algebraic system which is usually represented as a continuous-time state space model [4]. Considering that ASM requires a scalar function with domain as parameters and range as active or reactive power, in this section, we parameterize the WECC CMLD in a discretization manner. The parameterized model produces similar responses as the original one with high-fidelity as long as the Nyquist-Shannon sampling theorem is satisfied.

C. Parameterized WECC CMLD

The WECC CMLD is a hybrid model with dynamic and static components. The state vector $\boldsymbol{x} \in \mathbb{R}^{n_d}$ of three-phase motors and DER is governed by the following differential equation

$$\dot{\boldsymbol{x}}(t) = \boldsymbol{f}(\boldsymbol{x}(t), \boldsymbol{\theta}(t), \boldsymbol{u}(t)), \tag{1}$$

where $\boldsymbol{\theta}(t) \in \mathbb{R}^{n_p}$ denotes the parameter vector; $\boldsymbol{u}(t) = [|V(t)|, \phi(t), \Delta f(t)]^T$ is the input vector consisting of voltage magnitude, voltage angle and frequency deviation, respectively; $\boldsymbol{f} : \mathbb{R}^{n_d} \times \mathbb{R}^{n_p} \times \mathbb{R}^3 \rightarrow \mathbb{R}^{n_d}$ represents the dynamic model of three-phase motors, and DER; n_d and n_p are the total number of dynamic states and parameters. The active and reactive power output of the dynamic components, $\boldsymbol{y}_d(t) = [P_d(t), Q_d(t)]^T$ is given by

$$\boldsymbol{y}_d(t) = \boldsymbol{g}_d(\boldsymbol{x}(t), \boldsymbol{\theta}(t), \boldsymbol{u}(t)). \tag{2}$$

In PR using ASM, a mapping between parameters and active/reactive power is required for PR. Based on the fact that the input of load model $\boldsymbol{u}$ is usually sampled every T seconds, we can discretize (1) as

$$\boldsymbol{x}(k) = \bar{\boldsymbol{f}}(\boldsymbol{x}(k-1), \boldsymbol{\theta}(k-1), \boldsymbol{u}(k-1)), \tag{3}$$

where $\bar{\boldsymbol{f}}$ is the discretized function of $\boldsymbol{f}$, $k = 1, 2, \ldots, N$, N is the total number of measurements. Note that the sampling rate should satisfy Nyquist-Shannon sampling theorem to guarantee that discrete sequence of samples can capture all the information from a continuous-time signal. Then, $\boldsymbol{x}(k)$ can be calculated from the initial state $\boldsymbol{x}(0)$ by iteratively evaluating $\bar{\boldsymbol{f}}$ using past sequences of parameters and inputs, $[\boldsymbol{\theta}(k-1), \ldots, \boldsymbol{\theta}(0), \boldsymbol{u}(k-1), \ldots, \boldsymbol{u}(0)]$. Finally, by substituting (3) iteratively into (2), we can obtain the desired mapping using some algebraic function $\bar{\boldsymbol{g}}_d$:

$$\boldsymbol{y}_d(k) = \bar{\boldsymbol{g}}_d(\boldsymbol{\theta}(k), \ldots, \boldsymbol{\theta}(0), \boldsymbol{u}(k), \ldots, \boldsymbol{u}(0), \boldsymbol{x}(0)). \tag{4}$$

Regarding $\boldsymbol{x}$ and $\boldsymbol{u}$ as constants, Eq. (4) depicts the relationship between active/reactive power of dynamic components and parameters.

As for the static components such as single-phase motor, electronic load, and static ZIP load, the mapping from parameters to active and reactive power outputs can be represented as

$$\boldsymbol{y}_s(k) = \boldsymbol{g}_s(\boldsymbol{\theta}(k), \boldsymbol{u}(k)). \tag{5}$$

The total power output $\boldsymbol{y}(k)$ of the WECC CMLD can be calculated by adding the dynamic and static parameterized model together. For ease of deriving PR approach for the composite load model, we define the parameterized model as $\boldsymbol{g}$ in the form of

$$\begin{aligned} \boldsymbol{y}(k) &= \boldsymbol{y}_d(k) + \boldsymbol{y}_s(k) \\ &= \boldsymbol{g}(\boldsymbol{\theta}(k), \ldots, \boldsymbol{\theta}(0), \boldsymbol{u}(k), \ldots, \boldsymbol{u}(0), \boldsymbol{x}(0)). \end{aligned} \tag{6}$$

If the parameters are considered as time-invariant during a short time period, Eq. (6) can be simplified as

$$\boldsymbol{y}(k) = \boldsymbol{g}(\boldsymbol{\theta}, \boldsymbol{u}(k), \ldots, \boldsymbol{u}(0), \boldsymbol{x}(0)). \tag{7}$$

where $\boldsymbol{y}(k) = [P(k), Q(k)]^T$, and $\boldsymbol{g} = [g_P, g_Q]^T$.

III. PR Approach for WECC CMLD using ASM

In this section, we will use ASM to reduce the parameters of the WECC CMLD. Firstly, the preliminaries of ASM are introduced. Then, the application of ASM to WECC CMLD is elaborated in steps. Finally, the factors affecting the accuracy of PR is analyzed theoretically.

A. Preliminaries of ASM

An active subspace is a lower-dimensional linear subspace of the parameter space, along which input perturbations alter the model's predictions more than the perturbations along the directions which are orthogonal to the subspace on average. This subspace allows for a global measurement of sensitivity of output variables with respect to parameters, and is often used to decrease the dimension of the parameter space. Consider a parameterized function $g : \chi \to \mathbb{R}$ that maps the parameters of a system, $\bar{\boldsymbol{\theta}} \in \chi := \{\boldsymbol{x} \in \mathbb{R}^m | -1 \leqslant x_i \leqslant 1, i = 1, \ldots, m\}$, to a scalar output of interest, e.g., active power P or reactive power Q, where χ indicates a normalized set of parameter values.

To discover the active subspace, we define the following $\boldsymbol{C}$ matrix,

$$\boldsymbol{C} = \int_{\chi} (\nabla_{\bar{\boldsymbol{\theta}}} g(\bar{\boldsymbol{\theta}}))(\nabla_{\bar{\boldsymbol{\theta}}} g(\bar{\boldsymbol{\theta}}))^T \rho(\bar{\boldsymbol{\theta}}) \mathrm{d}\bar{\boldsymbol{\theta}}. \tag{8}$$

where $\rho(\bar{\boldsymbol{\theta}}) : \chi \to \mathbb{R}_+$ is the joint probability function of parameters satisfying

$$\int_{\chi} \rho(\bar{\boldsymbol{\theta}}) \mathrm{d}\bar{\boldsymbol{\theta}} = 1. \tag{9}$$

For any smooth function $g(\bar{\boldsymbol{\theta}})$, the matrix $\boldsymbol{C}$ is called *average derivative functional* in the context of dimension reduction, which weights input values according to the density $\rho(\bar{\boldsymbol{\theta}})$. Note that a single normalized parameter is a random variable taking values in $[-1, 1]$, which when appropriately scaled represents a parameter in the original model (7). Since the dimension of the parameter space in this model is 64, we take $m = 64$ throughout. The matrix $\boldsymbol{C}$ is the average of the outer product of the gradient of $g(\bar{\boldsymbol{\theta}})$ with itself and has some useful properties that will allow us to deduce information about how $g(\bar{\boldsymbol{\theta}})$ is altered by perturbations in its arguments.

Remark 1: From (8), each element of $\boldsymbol{C}$ is the average of the product of partial derivatives (which can be regarded as parameter sensitivity)

$$C_{ij} = \int_{\chi} \left(\frac{\partial g}{\partial \bar{\theta}_i}\right) \left(\frac{\partial g}{\partial \bar{\theta}_j}\right) \rho \mathrm{d}\bar{\boldsymbol{\theta}}, \quad i, j = 1, \ldots, m, \tag{10}$$

where C_{ij} is the (i, j) element of $\boldsymbol{C}$, and m is the number of parameters. If we consider $\nabla_{\bar{\boldsymbol{\theta}}} g(\bar{\boldsymbol{\theta}})$ to be a random vector by virtue of $\bar{\boldsymbol{\theta}}$'s density ρ, then $\boldsymbol{C}$ is the *uncentered covariance matrix* of the gradient of output with respect to the parameters [24]. This allows us to use the covariance matrix $\boldsymbol{C}$ to measure the correlation between each pair of parameter gradients. For simplicity, denote $\frac{\partial g}{\partial \theta_i}$ as s_i, denote the mean and standard deviation of gradient of ith parameter as μ_{s_i} and σ_{s_i}, respectively. Then, the correlation between (i, j) parameter gradients is

$$\begin{aligned} \rho_{s_i, s_j} &= \frac{\mathrm{cov}(s_i, s_j)}{\sigma_{s_i} \sigma_{s_j}} \\ &= \frac{\mathbb{E}\left[(s_i - \mu_{s_i})(s_j - \mu_{s_j})\right]}{\sigma_{s_i} \sigma_{s_j}} \\ &= \frac{C_{ij} - \mu_{s_i} \mu_{s_j}}{\sigma_{s_i} \sigma_{s_j}}. \end{aligned} \tag{11}$$

Eq. (11) shows that the $\boldsymbol{C}$ matrix encodes the correlation information between parameter gradients, which means the ASM takes into consideration the interdependency of parameters. This is one of the advantages compared to other PR methods.

The matrix $\boldsymbol{C}$ is symmetric, and thus permitting the spectral eigendecomposition

$$\boldsymbol{C} = \boldsymbol{W} \boldsymbol{\Lambda} \boldsymbol{W}^T. \tag{12}$$

where $\boldsymbol{W}$ is an orthogonal matrix whose columns $\boldsymbol{w}_i, (i = 1, \ldots, m)$ are the orthonormal eigenvectors of $\boldsymbol{C}$. $\boldsymbol{\Lambda} = \mathrm{diag}([\lambda_1, \ldots, \lambda_m])$, and $\lambda_1 \geqslant, \ldots, \geqslant \lambda_m$.

Since $\boldsymbol{W}$ is orthogonal, from the definition of eigenvectors and (8), the eigenvalues of $\boldsymbol{C}$ can be calculated as

$$\begin{aligned} \lambda_i &= \boldsymbol{w}_i^T \boldsymbol{C} \boldsymbol{w}_i \\ &= \boldsymbol{w}_i^T \left(\int_{\chi} (\nabla_{\bar{\boldsymbol{\theta}}} g(\bar{\boldsymbol{\theta}}))(\nabla_{\bar{\boldsymbol{\theta}}} g(\bar{\boldsymbol{\theta}}))^T \rho(\bar{\boldsymbol{\theta}}) \mathrm{d}\bar{\boldsymbol{\theta}} \right) \boldsymbol{w}_i \\ &= \int_{\chi} ((\nabla_{\bar{\boldsymbol{\theta}}} g(\bar{\boldsymbol{\theta}}))^T \boldsymbol{w}_i)^2 \rho(\bar{\boldsymbol{\theta}}) \mathrm{d}\bar{\boldsymbol{\theta}}, \quad i = 1, \ldots, m. \end{aligned} \tag{13}$$

From (13) we see that the eigenvalues of the $\boldsymbol{C}$ matrix are the mean squared directional derivatives of $g(\bar{\boldsymbol{\theta}})$ in the direction of the corresponding eigenvector. If an eigenvalue is small, then (13) shows that $g(\bar{\boldsymbol{\theta}})$ is insensitive in the direction of the corresponding eigenvector on average. On the contrary, a large eigenvalue indicates that $g(\bar{\boldsymbol{\theta}})$ changes significantly in the direction of the corresponding eigenvector.

After determining the eigendecomposition (12), the eigenvalues and eigenvectors can be separated according to the magnitudes of eigenvalues:

$$\boldsymbol{\Lambda} = \begin{bmatrix} \boldsymbol{\Lambda}_1 & 0 \\ 0 & \boldsymbol{\Lambda}_2 \end{bmatrix}, \quad \boldsymbol{W} = \begin{bmatrix} \boldsymbol{W}_1 & 0 \\ 0 & \boldsymbol{W}_2 \end{bmatrix} \tag{14}$$

where $\boldsymbol{\Lambda}_1$ and $\boldsymbol{W}_1$ contain the first n larger eigenvalues and corresponding eigenvectors, $\boldsymbol{\Lambda}_2$ and $\boldsymbol{W}_2$ contain the other $m - n$ smaller ones. To determine such separation, one can find the spectral gap between the nth and $(n + 1)$th eigenvalues on a log plot in the order of magnitudes. It is worth noting that the existence of a significant spectral gap directly indicates the existence of active subspace [24].

Keeping in mind that $\boldsymbol{W}$ is orthogonal, from (14), any parameter vector $\boldsymbol{\theta}$ can be represented as

$$\begin{aligned} \boldsymbol{\theta} &= \boldsymbol{W} \boldsymbol{W}^T \boldsymbol{\theta} \\ &= \boldsymbol{W}_1 \boldsymbol{W}_1^T \boldsymbol{\theta} + \boldsymbol{W}_2 \boldsymbol{W}_2^T \boldsymbol{\theta} \\ &= \boldsymbol{W}_1 \boldsymbol{\theta}_1 + \boldsymbol{W}_2 \boldsymbol{\theta}_2 \end{aligned} \tag{15}$$

Then, an output of interest with any parameter vector $\boldsymbol{\theta}$ is

$$g(\boldsymbol{\theta}) = g(\boldsymbol{W}_1 \boldsymbol{\theta}_1 + \boldsymbol{W}_2 \boldsymbol{\theta}_2). \tag{16}$$

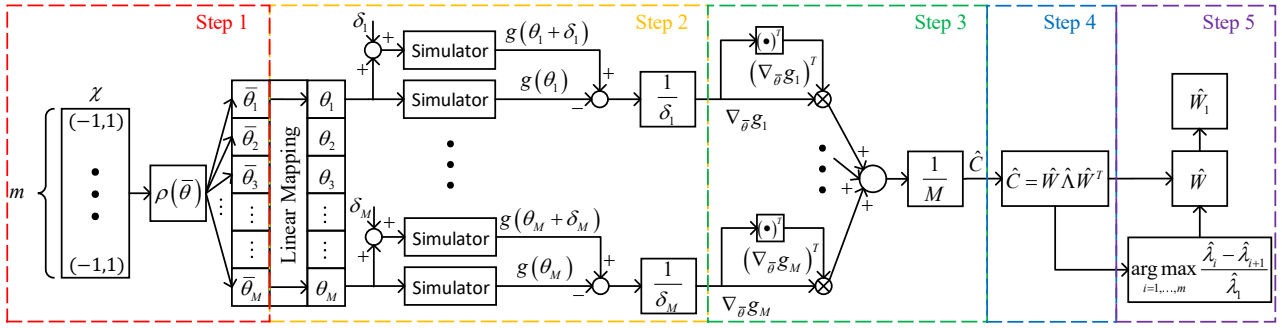

Fig. 2. The block diagram of the proposed PR algorithm based on ASM.

From the definition of $\boldsymbol{W}_1$ and $\boldsymbol{W}_2$, we know that small perturbations on $\boldsymbol{\theta}_2$ have low impact on the value of g. Conversely, small perturbations on $\boldsymbol{\theta}_1$ will alter g significantly. According to this property, the range of $\boldsymbol{W}_1$ is defined as the *active subspace*, and on the contrary, the range of $\boldsymbol{W}_2$ as the corresponding inactive subspace of the model. These subspaces describe the sensitivity of the output of interest with respect to parameter variations.

It is worth noting that, though both ASM and principal components analysis (PCA) include the process of eigendecomposition, they are intrinsically different. The PCA eigendecomposed the covariance matrix of the parameter vector $\boldsymbol{\theta}$, whereas the matrix to be eigendecomposed in the active subspace is defined as (8).

B. PR Algorithm based on ASM

The overall algorithm for PR of WECC CMLD using ASM is summarized in Fig. 2. The key idea of the algorithm is elaborated in details as follows:

Step 1: Construct the parameter set $\chi = [-1, 1]^m, m = 64$ as the normalized parameter space for all the selected parameters of WECC CMLD, and draw M samples $\{\bar{\boldsymbol{\theta}}_j\}, j = 1, \ldots, M$ from χ according to some probability density function satisfying (9). Usually, uniform distribution is chosen for simplicity.

Step 2: For each sampled parameter vector $\bar{\boldsymbol{\theta}}_j$, approximate the gradient $\nabla_{\bar{\boldsymbol{\theta}}} g_j = \nabla_{\bar{\boldsymbol{\theta}}} g(\bar{\boldsymbol{\theta}}_j)$ using first order forward finite differences method as follows:

$$\nabla_{\bar{\boldsymbol{\theta}}} g(\bar{\boldsymbol{\theta}}_j) = \begin{bmatrix} \frac{\partial g}{\partial \bar{\theta}_{j,1}} \\ \vdots \\ \frac{\partial g}{\partial \bar{\theta}_{j,m}} \end{bmatrix} \approx \begin{bmatrix} \frac{g(\theta_{j,1}+\boldsymbol{\delta}_{j,1}) - g(\theta_{j,1})}{\delta_{j,1}} \\ \vdots \\ \frac{g(\theta_{j,m}+\boldsymbol{\delta}_{j,m}) - g(\theta_{j,m})}{\delta_{j,m}} \end{bmatrix}, \; j = 1, \ldots, M, \tag{17}$$

where $\boldsymbol{\delta}_j$ is an arbitrarily small positive vector perturbation from the sampled parameter values. When g is a practical system, e.g., WECC CMLD, one needs to transform the normalized parameter vector $\bar{\boldsymbol{\theta}}_j$ to $\boldsymbol{\theta}_j$ that is in the standard range of parameters, using the following linear mapping,

$$\boldsymbol{\theta}_j = \frac{1}{2}(\mathrm{diag}(\boldsymbol{\theta}_{\mathrm{upper}} - \boldsymbol{\theta}_{\mathrm{lower}})\bar{\boldsymbol{\theta}}_j + (\boldsymbol{\theta}_{\mathrm{upper}} - \boldsymbol{\theta}_{\mathrm{lower}})). \tag{18}$$

where $\boldsymbol{\theta}_{\mathrm{upper}}$ and $\boldsymbol{\theta}_{\mathrm{lower}}$ are upper and lower bounds of the parameter vectors, respectively. Thus, $\boldsymbol{\theta}_j$ in (18) denotes the vector of real parameter values of the WECC CMLD.

Step 3: Approximate the average derivative functional $\boldsymbol{C}$ using Monte Carlo simulation as

$$\boldsymbol{C} = \hat{\boldsymbol{C}} \approx \frac{1}{M} \sum_{j=1}^{M} (\nabla_{\bar{\boldsymbol{\theta}}} g_j)(\nabla_{\bar{\boldsymbol{\theta}}} g_j)^T. \tag{19}$$

Step 4: Compute the eigendecomposition of approximate matrix $\hat{\boldsymbol{C}}$:

$$\hat{\boldsymbol{C}} = \hat{\boldsymbol{W}} \hat{\boldsymbol{\Lambda}} \hat{\boldsymbol{W}}^T, \tag{20}$$

which is equivalent to calculating the singular value decomposition of the matrix

$$\frac{1}{\sqrt{M}} [\nabla_{\bar{\boldsymbol{\theta}}} g_1, \ldots, \nabla_{\bar{\boldsymbol{\theta}}} g_M] = \hat{\boldsymbol{W}} \sqrt{\hat{\boldsymbol{\Lambda}}} \hat{\boldsymbol{V}}^T, \tag{21}$$

where the singular values are the square roots of the eigenvalues of $\hat{\boldsymbol{C}}$ and the left singular vectors are the eigenvectors of $\hat{\boldsymbol{C}}$. The singular value decomposition perspective was first used in [29] to determine the active subspace that is related to the principal components of a collection of gradients.

Step 5: After the decomposition (21), one needs to search for the largest spectral gap among eigenvalues in $\hat{\boldsymbol{\Lambda}}$ for subspace separation. The existence of a larger spectral gap indicates a more accurate determination of active subspace. To automatically find the optimal separation, we can use the following equation,

$$\Delta \hat{\lambda}_i = \frac{\hat{\lambda}_i - \hat{\lambda}_{i+1}}{\hat{\lambda}_1}, \; i = 1, \ldots, m-1. \tag{22}$$

Then, the dimension of the active subspace is

$$\dim(\mathrm{range}(\boldsymbol{W}_1)) = \underset{i=1,\ldots,m-1}{\mathrm{argmax}} \; \Delta \hat{\lambda}_i. \tag{23}$$

From (23), we know that the index of the largest value of $\Delta \hat{\lambda}_i$ indicates the location of the largest spectral gap. In the dimension reduction context, often only the first value $\Delta \hat{\lambda}_1$ is considered such that the dimension of the active subspace is limited to one, which makes it more convenient for visualization of the output as a function of the active subspace [24]. Then, the magnitudes of elements in the first eigenvector describe the weights of parameters.

Remark 2: The active subspace describes the most sensitive direction in the parameter space along which the output of interest evolves fastest. Thus, from (16) the output of

parameterized model can be approximated by only the active subspace of parameter space, i.e.,

$$g(\boldsymbol{\theta}) \approx g(\boldsymbol{W}_1\boldsymbol{\theta}_1),\ \boldsymbol{\theta}_1 = \boldsymbol{W}_1^T\boldsymbol{\theta}. \tag{24}$$

Eq. (24) indicates that g is related to $\boldsymbol{\theta}_1$ which is a linear combination of original parameters $\boldsymbol{\theta}$. This linear combination reflects the weight of each parameter and their collective influence on the output of interest.

The accuracy of the approximation (24) depends mainly on two factors which will be further discussed in the next subsection.

C. Accuracy Analysis of PR Based on ASM

In this subsection, two main factors affecting the accuracy of PR using ASM introduced above will be discussed.

1) Sample size M: In the above algorithm, the most costly computation processes are eigendecomposition and computing gradient for M times. In our case, the number of parameters is $m = 64$, so the computational cost of eigendecomposition is negligible compared to the computation of gradient. Thus, the selection of M that is large enough for approximating $\boldsymbol{\Lambda}$ and $\boldsymbol{W}$ while minimizing the computational cost is of vital importance. To estimate the first n eigenvalues of matrix $\boldsymbol{C}$, the sample size M can be chosen as

$$M = \beta n \log(m), \tag{25}$$

where β is an oversampling factor, which is usually selected between 70 and 120. In the next section, we will verify that this range of β is sufficient in the PR of WECC CMLD by experiment. The logarithm term $\log(m)$ follows from the bounds in the theorem proposed in [29].

2) Gradient approximation: The WECC CMLD suffers from high nonlinearity and complexity that render it difficult to derive a closed-form expression of gradient of output of interest with respect to the parameters. In view of the simulating g is not too expensive nor too noisy and m is not too large, we can utilize finite difference method to estimate the gradient. We know that, a smaller $\boldsymbol{\delta}$ produces a more accurate approximation but with increased computational cost and vice versa. This relationship can be expressed as the following inequality by using (17),

$$\left\| \nabla_{\bar{\boldsymbol{\theta}}} g(\bar{\boldsymbol{\theta}}_j) - \frac{g(\boldsymbol{\theta}_j+\boldsymbol{\delta}_j) - g(\boldsymbol{\theta}_j)}{\boldsymbol{\delta}_j} \right\| \leqslant \sqrt{m}\alpha(\boldsymbol{\delta}_j),\ j = 1, \ldots, M, \tag{26}$$

where $\lim_{\boldsymbol{\delta}_j \to 0} \alpha(\boldsymbol{\delta}_j) = 0$.

In the following, we will give a criterion for the selection of finite difference perturbation $\boldsymbol{\delta}_j$ by restating Theorem 3.13 from [24].

Theorem 1 (Accuracy criterion of estimated active subspace [Thm. 3.13 in [24]]): Assume that $\left\|\nabla_{\bar{\boldsymbol{\theta}}} g(\bar{\boldsymbol{\theta}}_j)\right\| \leqslant L$ for $j = 1, \ldots, M$, and choose small parameter ε and β in (25) satisfying

$$0 < \varepsilon \leqslant \frac{\lambda_n - \lambda_{n+1}}{5\lambda_1}, \tag{27}$$

$$\beta \geqslant \max \frac{L^2}{n\varepsilon^2} \left\{ \frac{\lambda_1}{\lambda_n^2}, \frac{1}{\lambda_1} \right\}. \tag{28}$$

If the finite difference perturbation is small enough such that

$$5m\alpha(\boldsymbol{\delta}_j)^2 + 10L\sqrt{m}\alpha(\boldsymbol{\delta}_j) \leqslant \hat{\lambda}_n - \hat{\lambda}_{n+1},\ j = 1, \ldots, M, \tag{29}$$

then, the distance between real active subspace $\boldsymbol{W}_1$ and the approximated one $\hat{\boldsymbol{W}}_1$ using Monte Carlo and finite difference approximation method is bounded by

$$\begin{aligned} \operatorname{dist}(\operatorname{range}(\hat{\boldsymbol{W}}_1), \operatorname{range}(\boldsymbol{W}_1)) \leqslant & \frac{4m\alpha(\boldsymbol{\delta}_j)^2 + 8L\sqrt{m}\alpha(\boldsymbol{\delta}_j)}{(1-\varepsilon)\lambda_n - (1+\varepsilon)\lambda_{n+1}} \\ & + \frac{4\varepsilon\lambda_1}{\lambda_n - \lambda_{n+1}} \end{aligned} \tag{30}$$

for $j = 1, \ldots, M$, with high probability.

Proof: The proof follows the similar steps as in [24] by simply combining (25) and (28). ∎

We choose $\boldsymbol{\delta}_j = 1 \times 10^{-6}$, $L = 1$, $m = 64$, $\varepsilon = 0.1$, $\beta = 100$ and $\alpha(\boldsymbol{\delta}_j) = \boldsymbol{\delta}_j$ such that (27)-(29) hold. Then, based on Theorem 1, the error of active subspace estimate is bounded by 0.8 and the simulation result is not too far off.

Remark 2: When the two factors are appropriately set, another most influential factor is the normalized eigenvalue separation $\lambda_1/\lambda_n - \lambda_{n+1}$ in (30), which depends on the system characteristics only. The existence of significant spectral gap indicates a clear active subspace and accurate estimation.

IV. Case Studies

In this section, the proposed ASM is applied to analyze the sensitivities of the parameters of WECC CMLD. Firstly, a basic case study is conducted to show the implementation process and how to interpret the result. Then, the proposed method is also applied to the FIVDR case to show its effectiveness on more complicated voltage profile. Finally, three classical PR techniques are applied to the WECC CMLD for comparison with the proposed method.

A. Case I: Apply ASM to WECC CMLD and Result Analyses

1) Simulation Setup: We first provide the simulation setup for the case studies. The range of parameters $[\boldsymbol{\theta}_{\text{lower}}, \boldsymbol{\theta}_{\text{upper}}]$ is set by adding plus and minus fifty percent of perturbations on the standard values given in the guideline of WECC CMLD [28] as shown in Table I. Using (25) with $m = 64$, $n = 1$ and $\beta = 120$, the sample size is calculated as $M_{\text{ASM}} \approx 500$. In Section IV-C, we will show the convergence of parameter sensitivity with respect to increasing sample size, from which we can conclude that $M_{\text{ASM}} = 500$ is a good balance between accuracy and computational cost. Then, the samples are drawn uniformly from χ. When approximating the gradient using (17), the finite difference perturbation $\boldsymbol{\delta}$ is chosen as 1×10^{-6}, which is small enough to satisfy (29). Since ASM assumes scalar function g, we conduct the simulation by selecting active and reactive power as output of interest separately. The voltage and power measurements for PR in this simulation is generated by the Power System Simulator for Engineering (PSS/E) and the ACTIVSg500 test case with a line-to-ground fault [21] as shown in Fig. 3. The case study is conducted on a standard PC with an Intel(R) Xeon(R) CPU running at 3.70 GHz and with 32.0 GB of RAM using MATLAB.

TABLE I
NUMERICAL RANGE OF LOAD PARAMETERS OF WECC CMLD

Parameter	LB	UB	Parameter	LB	UB	Parameter	LB	UB	Parameter	LB	UB
Motor A			EtrqB	1	3	Np2	1.6	4.8	Trf	0.015	0.06
TpoA	0.046	0.184	DB	0.5	2.0	Nq1	1	4	Kqv	0.5	2.0
TppoA	0.001	0.004	Motor C			Nq2	1.25	5	Tp	0.01	0.04
LpA	0.05	0.20	TpoC	0.05	0.20	CmpKpf	0	2	Tiq	0.01	0.04
LppA	0.042	0.168	TppoC	0.0013	0.0052	CmpKqf	-6.6	-1.65	Tpord	2.5	10
LsA	0.9	3.6	LpC	0.08	0.32	Static Load			Kpg	50	200
RsA	0.02	0.08	LppC	0.06	0.24	P1c	0	0.4	Kig	5	20
HA	0.05	0.20	LsC	0.9	3.6	P2c	0	0.6	Tg	0.01	0.04
EtrqA	0.5	2.0	RsC	0.015	0.06	Q1c	0	0.4	Tv	0.01	0.04
DA	0.5	2.0	HC	0.1	0.4	Q2c	0	0.6	Xe	0.125	0.5
Motor B			EtrqC	1.8	2.2	Pfreq	-0.2	0.2	Load Fraction		
TpoB	0.05	0.20	DC	0.5	2.0	Qfreq	-2	-0.5	Fma	0	0.5
TppoB	0.0013	0.0052	Motor D			Electronic Load			Fmb	0	0.5
LpB	0.08	0.32	Kp1	0	1	Frcel	0	0.375	Fmc	0	0.5
LppB	0.06	0.24	Kp2	6	24	Vd1	0.5	1.5	Fmd	0	0.5
LsB	0.9	3.6	Kq1	3	12	Vd2	0.25	1	Fel	0	0.5
RsB	0.015	0.06	Kq2	5.5	22	DER_A			Fzip	0	0.5
HB	0.5	2.0	Np1	0.5	2	Trv	0.01	0.04	Fdg	-0.5	0

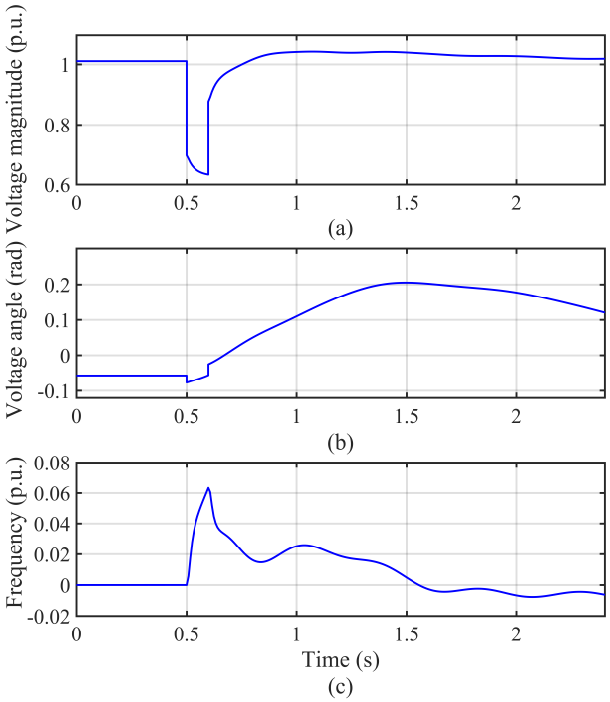

Fig. 3. The load bus input profile: (a) voltage magnitude; (b) voltage angle; (c) frequency.

2) Discovering Active Subspace and Parameter Sensitivities: To discover the active subspace, we can follow the algorithm provided in Section III.B. Given the simulation setup as above, we firstly approximate the matrix $\boldsymbol{C}$ by Monte Carlo simulation (19) for $M_{\text{ASM}} = 500$ with the gradient estimated by finite difference method (17). In this case study, the $g(\boldsymbol{\theta}_j+\boldsymbol{\delta}_j)$ and $g(\boldsymbol{\theta}_j)$ before transient are obtained using the mathematical model of WECC composite load developed in [30] for faster calculation of the gradient. Instead, one can also use other commercial software such as PSS/E or PSLF with potentially longer simulation time. Once the approximate $\hat{\boldsymbol{C}}$ is constructed, the singular value decomposition is applied to abstract the eigenvalues and corresponding eigenvectors. The eigenvalues of $\hat{\boldsymbol{C}}$ are shown in Fig. 4 in descending order. Recall that a significant spectral gap indicates the existence of active subspace, so it is important to look into the gaps of eigenvalues in Fig. 4. Note that the largest spectral gap exists between the first and second ones even though it seems that the one between the 45th and 46th ones is larger since it is a semilog plot. To clearly show the largest spectral gap, we conduct the normalized eigenvalue separation (22) and the result in Fig. 5 clearly shows the dominance of the gap between the first and second eigenvalues.

Then, the first eigenvector forms the active subspace of $\hat{\boldsymbol{C}}$ and the magnitude of each element of the eigenvector describes the sensitivity of each corresponding parameter and their interdependency. The weights of parameters with respect to the real and reactive power are shown in Fig. 6 and Fig. 7, respectively. The parameters in the red rectangles that have the largest weights imply the reduced parameter space. However, noting that the weights of parameters in the green rectangle though dominated by those in the red, are still larger than those that are almost zero. Thus, one may wonder whether these parameters also have significant impacts on the output of the interest as well. To verify the PR result, we will perform further studies in the following subsections.

3) Sufficient Summary Plot: In this subsection, we utilize sufficient summary plot to empirically validate the active subspace discovered in the last subsection. Sufficient summary plot was originally developed as a visualization tool for determining low-dimensional combination of inputs in regression graphics. In the context of PR, it is often used to verify the active subspace, because it reveals the relationship between the output of interest P or Q, and the *linear combination* of input parameters $\boldsymbol{W}_1^T\boldsymbol{\theta}_j$. If the relationship presents evidently tight and univariate trend, then one can conclude that the discovered active subspace is validated.

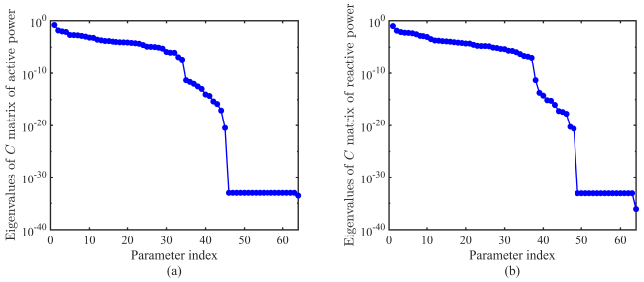

Fig. 4. The semilog plot of the magnitudes of eigenvalues of matrix $\hat{\boldsymbol{C}}$ with respect to (a) real power and (b) reactive power.

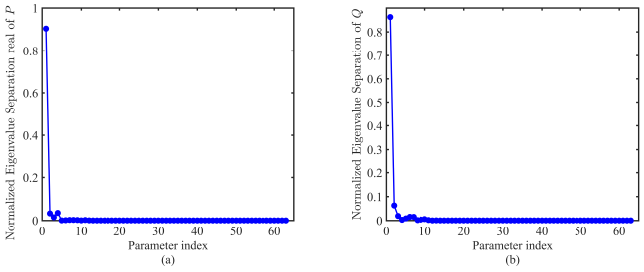

Fig. 5. The normalized eigenvalue separation of the magnitudes of eigenvalues of matrix $\hat{\boldsymbol{C}}$ with respect to (a) real power and (b) reactive power.

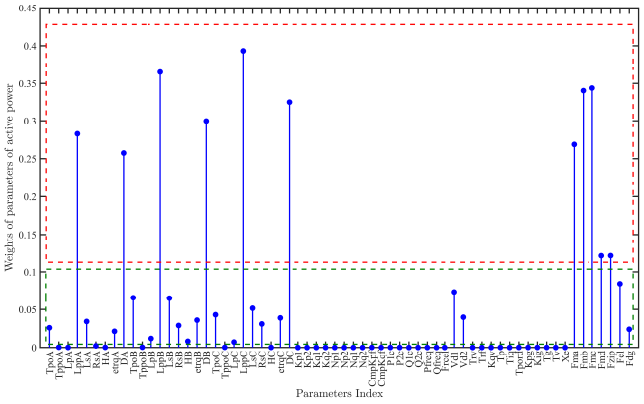

Fig. 6. The magnitudes of first eigenvector denoting the sensitivities of parameters of WECC CMLD with respect to real power.

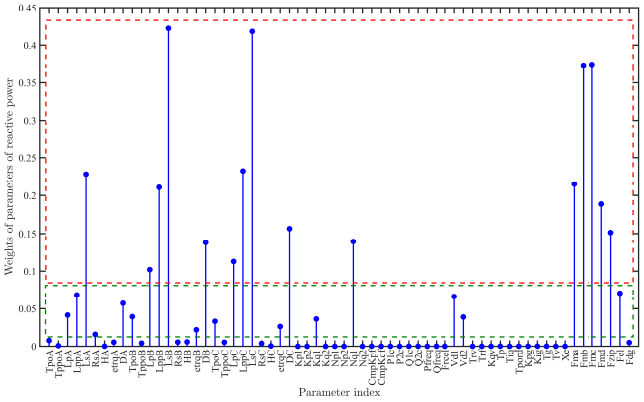

Fig. 7. The magnitudes of first eigenvector denoting the sensitivities of parameters of WECC CMLD with respect to reactive power.

Fig. 8 shows the sufficient summary plots of real and reactive power with respect to $\boldsymbol{W}_1^T\boldsymbol{\theta}_j$. The obvious linear trends verify the effectiveness of active subspace.

4) PR Result Validation: To finally determine the dimension of reduced parameter space, we conduct the following

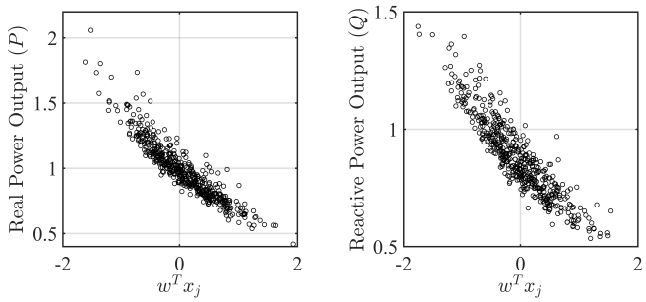

Fig. 8. Sufficient summary plots of (a) real and (b) reactive power with respect to the active subspace using $M_{\mathrm{ASM}} = 500$ samples.

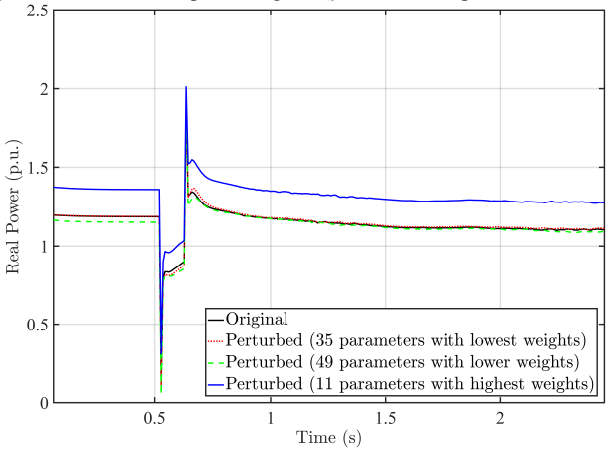

Fig. 9. Validation of PR result for real power of WECC CMLD, with different combinations of parameters perturbed by twenty percent.

simulations on the WECC CMLD. We first add 20% of positive perturbations to the insensitive parameters outside the red rectangles of Fig. 6 and Fig. 7. The results are shown as red lines in Fig. 9 and Fig. 10, respectively. Then, we add same perturbations to the parameters outside both rectangles to test whether restricting the PR result will lead to significant accuracy improvement. The results are shown in green dashed lines in Fig. 9 and Fig. 10. Finally, we add the same perturbations to the most sensitive parameters in the red rectangles, and the results are denoted in blue dotted lines.

From Fig. 9 and Fig. 10, we find that the real and reactive power are sensitive to the parameters inside the red rectangles and insensitive to the others. Moreover, including the parameters inside the green rectangles as sensitive ones does not have a noticeable impact on accuracy. Therefore, we can conclude that the parameters of the WECC CMLD can be reduced to the ones in the red rectangles only with almost the same dynamic response, which verifies the effectiveness of ASM.

B. Case II: Influence of FIDVR on Reduction Result

In this subsection, we will test the performance of the proposed method on FIDVR case which is obtained from real utility data, as shown in Fig. 11. This case contains multi-phase faults, including phase-to-phase, phase-to-phase-to-ground and three-phase-to-ground faults. The other simulation setup is the same as that in Case I.

Comparing the parameter sensitivity results in Fig. 12 and Fig. 13 with Case I, we can find that the parameters of single-phase motor become sensitive. This can be attributed to that

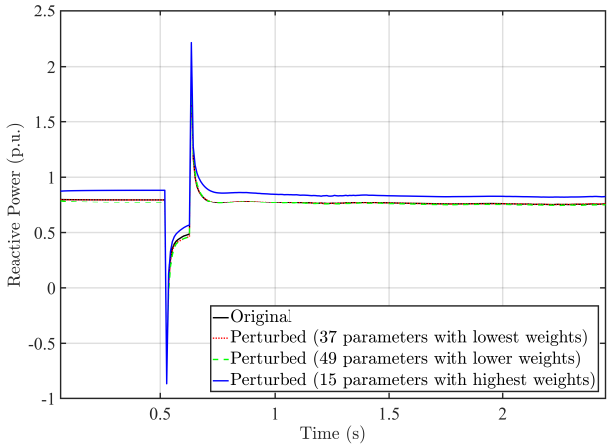

Fig. 10. Validation of PR result for reactive power of WECC CMLD, with different combinations of parameters perturbed by twenty percent.

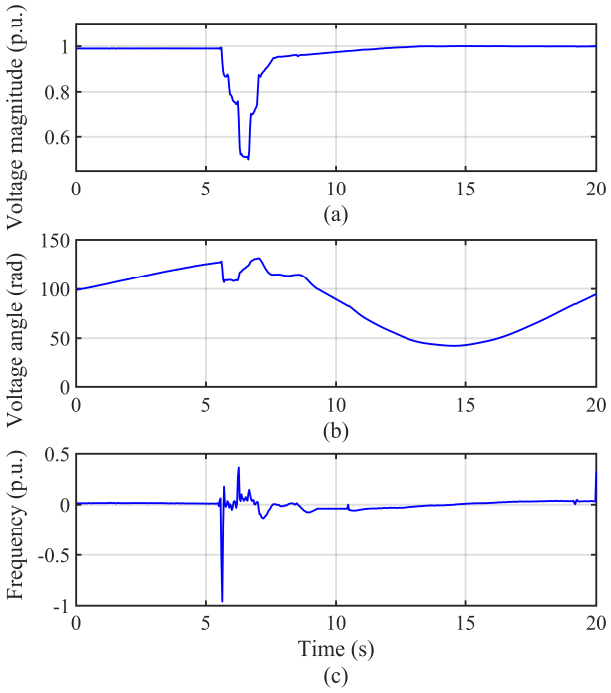

Fig. 11. The load bus input profile of FIDVR case: (a) voltage magnitude; (b) voltage angle; (c) frequency.

the single-phase motor plays an important role in capturing the dynamics during the delayed-recovery stage. Same as in Case I, 20% of perturbation is added to three parameter sets: parameters with lowest sensitivities (outside all the rectangles in Fig. 12 and Fig. 13), parameters with lower sensitivities (outside the red rectangles), and most sensitive parameters (inside the red rectangles). The comparison results in Fig. 14 and Fig. 15 show that the output of interest is altered significantly in the calculated sensitive direction but is almost not influenced when perturbing the insensitive parameters. This verifies the effectiveness of our method on FIDVR case.

C. Case III: Comparison with Three Classical PR methods

In this subsection, the proposed ASM method is compared with three representative and widely-used methods: FWKL method [21], Sobel method [17] and Morris method In [9]. The

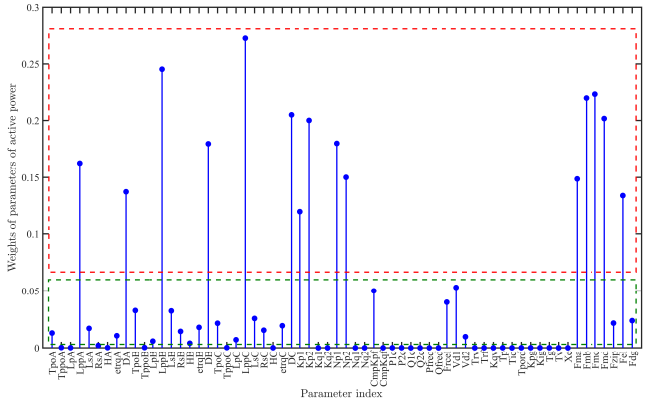

Fig. 12. The parameter sensitivities of WECC CMLD with respect to active power in FIDVR case.

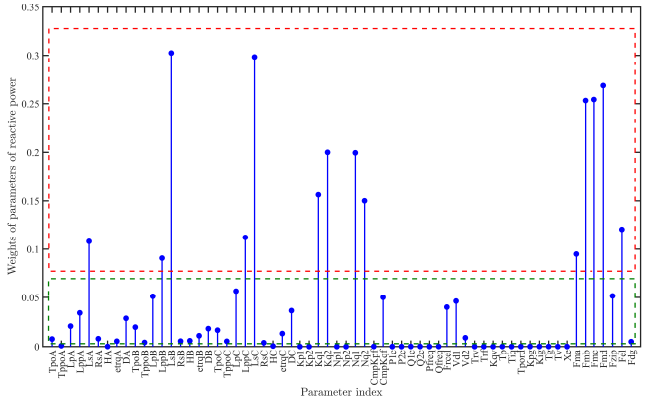

Fig. 13. The parameter sensitivities of WECC CMLD with respect to reactive power in FIDVR case.

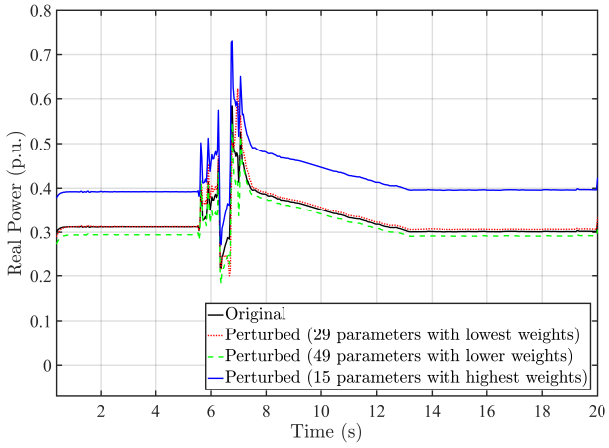

Fig. 14. Validation of PR result for real power of WECC CMLD, with different combinations of parameters perturbed by twenty percent

regularization parameter λ of FWKL is chosen as 100. The sample size of Monte Carlo simulation for Sobel method is selected as $M_{\text{Sobel}} = 1500$. The times of repetition for Morris method is selected as $M_{\text{Morris}} = 15$. The other simulation setups are the same as in Case I. Since the results of active and reactive power are consistent, for simplicity, only the results of active power are shown here.

The parameter sensitivities calculated by three methods are shown in Fig. 16-18, respectively. We can observe that, Morris method reduces least number of parameters, while Sobel method reduces the most. Moreover, the identified sensitive

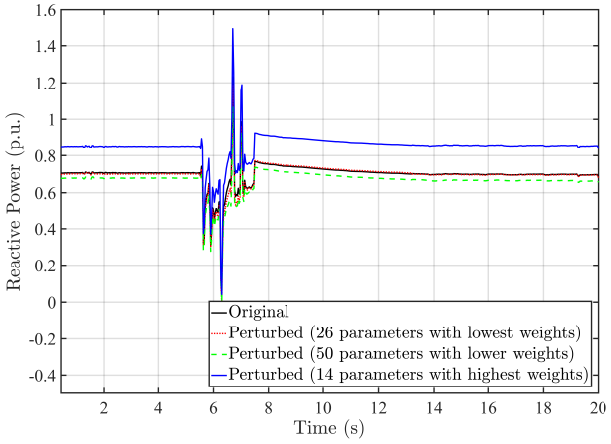

Fig. 15. Validation of PR result for reactive power of WECC CMLD, with different combinations of parameters perturbed by twenty percent.

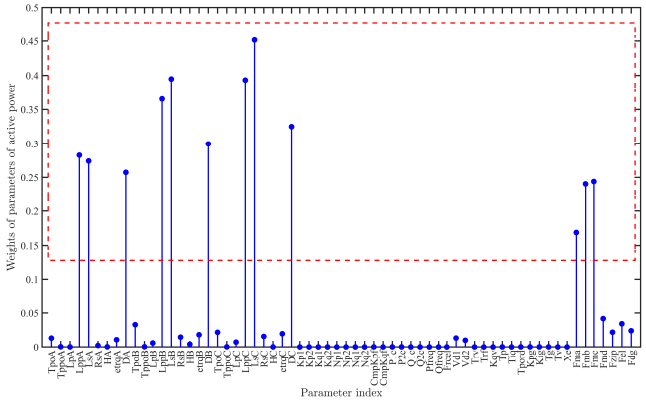

Fig. 16. Parameter sensitivities calculated by FWKL method. 12 parameters in the red rectangle are considered as sensitive ones.

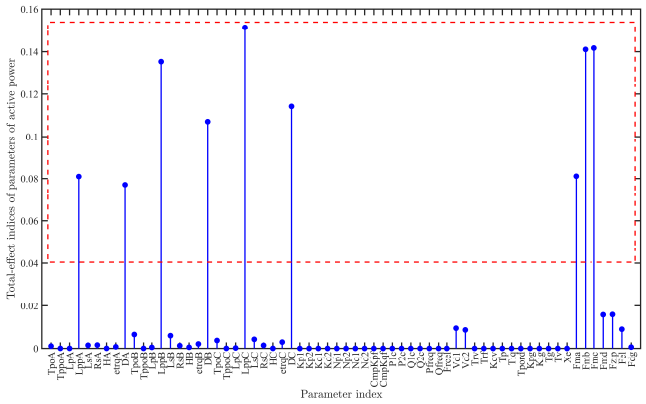

Fig. 17. Parameter sensitivities calculated by Sobel method. 9 parameters in the red rectangle are considered as sensitive ones.

parameter indices by Sobel are the most similar to those by ASM. The result validation is conducted by adding 20% on all sensitive and insensitive parameters sets, respectively. From Fig. 19, we can observe that, the blue line (ASM) deviates farthest away from the black line (original) in the sensitive direction, and is closest to that in the insensitive one. This indicates that ASM is the most accurate among the four methods for this case.

Some key features of the four methods can be concluded as Table. II. Note that the computational cost of ASM, Sobel and

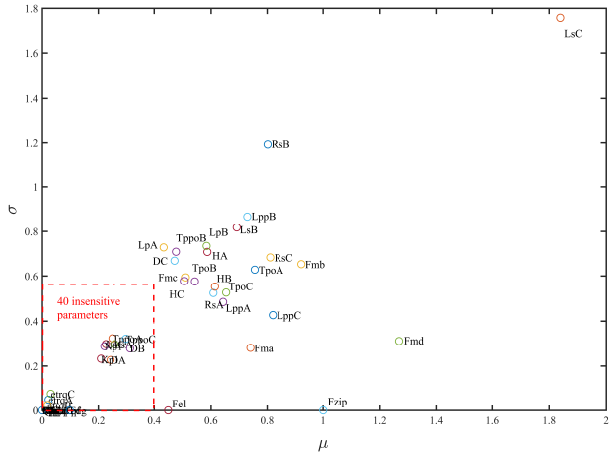

Fig. 18. Parameter sensitivities calculated by Morris method. 24 parameters outside the red rectangle are considered as sensitive ones. μ and σ are the mean and standard deviation of the elementary effects, respectively.

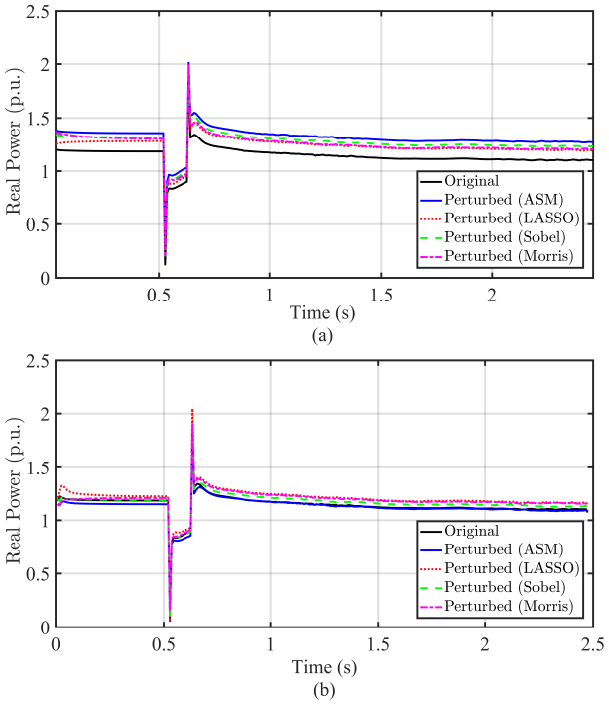

Fig. 19. Comparison of results validation of four methods by adding 20% perturbation on: (a) sensitive parameters; (b) insensitive parameters.

Morris are considered in terms of the number of experiments. FWKL is optimization-based, thus its computational cost depends on the numbers of both iterations and experiments, which makes it take more time than the other three methods. To further compare the computational cost of ASM and Sobel methods, we sequentially increase the Monte Carlo sample sizes to observe the converge rate of parameter sensitivities. Fig. 20 shows that the sensitivities obtained by ASM converge after 500 samples, while Sobel needs about 1500 ones. As a conclusion, the ASM is the most accurate with relatively lower computational cost (than Sobel and FWKL methods).

V. Conclusions

A novel PR approach for the WECC CMLD is proposed based on ASM. With this approach, the sensitivities of param-

TABLE II
COMPARISON OF KEY FEATURES OF THE FOUR PR METHODS.

	Category	Accuracy	Interaction	Computation
ASM	Gradient, Monte Carlo	Accurate	Quantitative	$2mM_{\mathrm{ASM}}$
FWKL	Optimization	Rough	Qualitative	Depends
Sobel	Variance, Monte Carlo	Accurate	Quantitative	$M_{\mathrm{Sobel}}(m+2)$
Morris	OAT	Rough	Qualitative	$M_{\mathrm{Morris}}(m+1)$

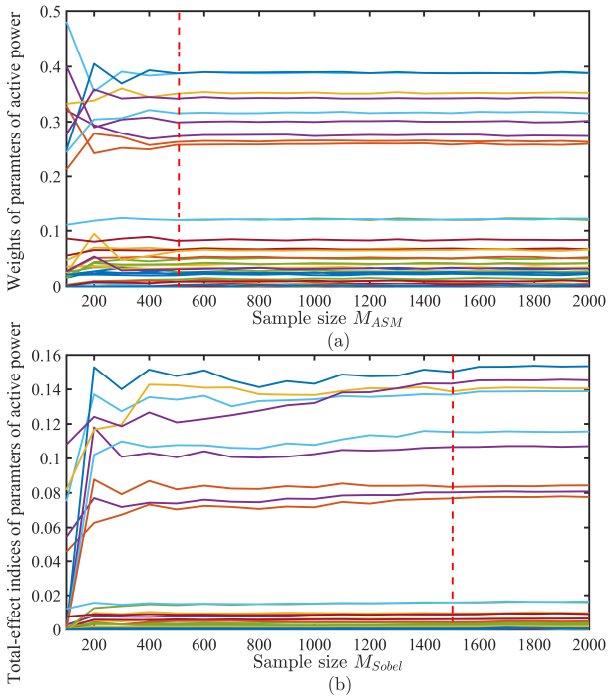

Fig. 20. Comparison of convergence rates of: (a) ASM; (b) Sobel.

eters are computed while the interdependency among the parameters is taken into consideration. By applying the proposed algorithm to the WECC CMLD, the dimensions of parameter spaces can be significantly reduced. The PR result is validated by sufficient summary plot and perturbation tests with different voltage cases. The comparison with other classical methods has shown the advantages of the proposed method.

Note that the ASM requires scalar function which limits its application to vector-valued parameterized model whose output is $[P, Q]^T$. Therefore, it cannot be directly used to analyze the parameter sensitivity for both real and reactive power simultaneously. One may use a scalar to combine them, however such output of interest may lack the physical meaning. We would like trying to extend the scalar ASM to deal with vector-valued functions in the future work.

REFERENCES

[1] K. Zhang, H. Zhu, and S. Guo, "Dependency analysis and improved parameter estimation for dynamic composite load modeling," *IEEE Trans. Power Syst.*, vol. 32, no. 4, pp. 3287–3297, Jul. 2017.

[2] C. Wang, Z. Wang, J. Wang, and D. Zhao, "Robust Time-Varying Parameter Identification for Composite Load Modeling," *IEEE Trans. Smart Grid*, vol. 10, no. 1, pp. 967–979, Jan. 2019.

[3] A. Arif, Z. Wang, J. Wang, B. Mather, H. Bashualdo, and D. Zhao, "Load ModelingA Review," *IEEE Trans. Smart Grid*, vol. 9, no. 6, pp. 5986–5999, Nov. 2018.

[4] Z. Ma, Z. Wang, D. Zhao, and B. Cui, "High-fidelity large-signal order reduction approach for composite load model," *IET Gener. Transm. Distrib.*, vol. 14, no. 21, pp. 4888–4897, Aug. 2020.

[5] Q. Huang, R. Huang, B. J. Palmer, Y. Liu, S. Jin, R. Diao, Y. Chen, and Y. Zhang, "A generic modeling and development approach for WECC composite load model," *Electr. Power Syst. Res.*, vol. 172, pp. 1–10, Jul. 2019.

[6] A. Saltelli, "Sensitivity analysis for importance assessment," *Risk Anal.*, vol. 22, no. 3, pp. 579–590, Jun. 2002.

[7] T. Homma and A. Saltelli, "Importance measures in global sensitivity analysis of nonlinear models," *Reliab. Eng. Syst. Saf.*, vol. 52, no. 1, pp. 1–17, Apr. 1996.

[8] S. Marino, I. B. Hogue, C. J. Ray, and D. E. Kirschner, "A methodology for performing global uncertainty and sensitivity analysis in systems biology," *J. Theor. Biol.*, vol. 254, no. 1, pp. 178 – 196, Sep. 2008.

[9] M. D. Morris, "Factorial sampling plans for preliminary computational experiments," *Technometrics*, vol. 33, no. 2, pp. 161–174, May 1991.

[10] D. K. Lin, "A new class of supersaturated designs," *Technometrics*, vol. 35, no. 1, pp. 28–31, Feb. 1993.

[11] A. Dean and S. Lewis, *Screening: methods for experimentation in industry, drug discovery, and genetics*. Springer Science & Business Media, 2006.

[12] B. Bettonvil and J. P. Kleijnen, "Searching for important factors in simulation models with many factors: Sequential bifurcation," *Eur. J. Oper. Res.*, vol. 96, no. 1, pp. 180–194, Jan. 1997.

[13] K. Hinkelmann and O. Kempthorne, *Design and analysis of experiments*. Wiley Online Library, 1994, vol. 1.

[14] B. Iooss and P. Lemaître, "A review on global sensitivity analysis methods," in *Uncertainty management in simulation-optimization of complex systems*. Springer, 2015, pp. 101–122.

[15] I. M. Sobol, "Global sensitivity indices for nonlinear mathematical models and their monte carlo estimates," *Math. Comput. Simul.*, vol. 55, no. 1-3, pp. 271–280, Feb. 2001.

[16] A. Saltelli, P. Annoni, I. Azzini, F. Campolongo, M. Ratto, and S. Tarantola, "Variance based sensitivity analysis of model output. design and estimator for the total sensitivity index," *"Comput. Phys. Commun.*, vol. 181, no. 2, pp. 259–270, Feb. 2010.

[17] A. Saltelli, M. Ratto, T. Andres, F. Campolongo, J. Cariboni, D. Gatelli, M. Saisana, and S. Tarantola, *Global sensitivity analysis: the primer*. John Wiley & Sons, 2008.

[18] A. Saltelli and P. Annoni, "How to avoid a perfunctory sensitivity analysis," *Environ. Model. Softw.*, vol. 25, no. 12, pp. 1508–1517, Dec. 2010.

[19] H. Scheffe, *The analysis of variance*. John Wiley & Sons, 1999.

[20] A. Saltelli and R. Bolado, "An alternative way to compute fourier amplitude sensitivity test (FAST)," *Compu. Stat. Data An.*, vol. 26, no. 4, pp. 445 – 460, Feb. 1998.

[21] F. Bu, Z. Ma, Y. Yuan, and Z. Wang, "WECC composite load model parameter identification using evolutionary deep reinforcement learning," *IEEE Trans. Smart Grid*, vol. 11, no. 6, pp. 5407–5417, Jul. 2020.

[22] J.-Y. Tissot and C. Prieur, "Bias correction for the estimation of sensitivity indices based on random balance designs," *Reliab. Eng. Syst. Safe.*, vol. 107, pp. 205 – 213, Nov. 2012.

[23] J. Ma, D. Han, R.-M. He, Z.-Y. Dong, and D. J. Hill, "Reducing identified parameters of measurement-based composite load model," *IEEE Trans. Power Syst.*, vol. 23, no. 1, pp. 76–83, Jan. 2008.

[24] P. G. Constantine, *Active subspaces: Emerging ideas for dimension reduction in parameter studies*. SIAM-Society for Industrial and Applied Mathematics, 2015.

[25] T. Loudon and S. Pankavich, "Mathematical analysis and dynamic active subspaces for a long term model of hiv," *Math Biosci Eng*, vol. 14, no. 3, pp. 709–733, Jun. 2016.

[26] P. Constantine, M. Emory, J. Larsson, and G. Iaccarino, "Exploiting active subspaces to quantify uncertainty in the numerical simulation of the hyshot ii scramjet," *J. Comput. Phys.*, vol. 302, pp. 1 – 20, Dec. 2015.

[27] "The new aggregated distributed energy resources (DER_A) model for transmission planning studies: 2019 update," Electrical Power Research Institute (EPRI), Tech. Rep., 2019.

[28] "Technical reference document: dynamic load modeling," North American Reliability Cooperation, Tech. Rep., 2016.

[29] T. M. Russi, "Uncertainty quantification with experimental data and complex system models," Ph.D. dissertation, UC Berkeley, 2010.

[30] Z. Ma, Z. Wang, Y. Wang, R. Diao, and D. Shi, "Mathematical representation of the WECC composite load model," *J. Modern Power Syst. Clean Energy*, vol. 8, no. 5, pp. 1015–1023, Aug. 2019.

Zixiao Ma (S'18) is currently a Ph.D. student in the Department of Electrical and Computer Engineering at the Iowa State University, Ames, IA, USA. He received his B.S. degree in Automation and M.S. degree in Control theory and Control Engineering from Northeastern University in 2014 and 2017 respectively. His research interests are focused on the power system load modeling, microgrids, nonlinear control and model reduction.

Bai Cui (S'15–M'18) received the Ph.D. degrees in electrical and computer engineering from the Georgia Institute of Technology in 2018. He is a researcher with the National Renewable Energy Laboratory (NREL). Prior to joining NREL, he was a postdoctoral appointee with Argonne National Laboratory from 2018 to 2019. His research interests include control and optimization problems in power systems. His research interests include voltage/var control, renewable energy integration, distribution system optimization and control, and power system protection.

Zhaoyu Wang (S13-M15-SM20) is the Harpole-Pentair Assistant Professor with Iowa State University. He received the B.S. and M.S. degrees in electrical engineering from Shanghai Jiaotong University, and the M.S. and Ph.D. degrees in electrical and computer engineering from Georgia Institute of Technology. His research interests include optimization and data analytics in power distribution systems and microgrids. He is the Principal Investigator for a multitude of projects focused on these topics and funded by the National Science Foundation, the Department of Energy, National Laboratories, PSERC, and Iowa Economic Development Authority. Dr. Wang is the Chair of IEEE Power and Energy Society (PES) PSOPE Award Subcommittee, Co-Vice Chair of PES Distribution System Operation and Planning Subcommittee, and Vice Chair of PES Task Force on Advances in Natural Disaster Mitigation Methods. He is an editor of IEEE Transactions on Power Systems, IEEE Transactions on Smart Grid, IEEE Open Access Journal of Power and Energy, IEEE Power Engineering Letters, and IET Smart Grid. Dr. Wang has been a recipient of the National Science Foundation (NSF) CAREER Award, the IEEE PES Outstanding Young Engineer Award, and the Harpole-Pentair Young Faculty Award Endowment.

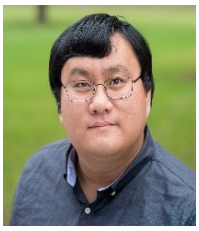

Dongbo Zhao (SM16) received his B.S. degrees from Tsinghua University, Beijing, China, the M.S. degree from Texas A&M University, College Station, Texas, and the Ph.D degree from Georgia Institute of Technology, Atlanta, Georgia, all in electrical engineering. He has worked with Eaton Corporation from 2014 to 2016 as a Lead Engineer in its Corporate Research and Technology Division, and with ABB in its US Corporate Research Center from 2010 to 2011. Currently he is a Principal Energy System Scientist with Argonne National Laboratory, Lemont, IL. He is also an Institute Fellow of Northwestern Argonne Institute of Science and Engineering of Northwestern University. His research interests include power system control, protection, reliability analysis, transmission and distribution automation, and electric market optimization.

Dr. Zhao is a Senior Member of IEEE, and a member of IEEE PES, IAS and IES Societies. He is the editor of IEEE Transactions on Power Delivery, IEEE Transactions on Sustainable Energy, and IEEE Power Engineering Letters. He is the subject editor of subject Power system operation and planning with renewable power generation of IET Renewable Power Generation and the Associate Editor of IEEE Access.